Materials Today: Proceedings xxx (xxxx) xxx

Contents lists available at ScienceDirect

Materials Today: Proceedings

journal homepage: www.elsevier.com/locate/matpr

Simple Co-precipitation synthesis and characterization of magnetic spinel $NiFe_2O_4$ nanoparticles

Subiya Kazi [a], Shaukatali Inamdar [b], Yuvraj sarnikar [c], Dhanraj Kamble [d], Radhakrishnan Tigote [a,*]

[a] Department of Chemistry, Dr. Babasaheb Ambedkar Marathwada University, Sub campus Osmanabad, Maharashtra 413 501, India
[b] Department of Pharmaceutical Chemistry, College of Health Sciences, University of KwaZulu-Natal (Westville), Durban 4000, South Africa
[c] Department of Chemistry, Dayanand Science College Latur, Maharashtra 413 531, India
[d] Department of Chemistry, S.B.E.S. College of Science, Aurangabad, India

ARTICLE INFO

Article history:
Available online xxxx

Keywords:
Ni-ferrite Nanoparticles
Band Gap
Size and Shape
Magnetic Properties
Co-precipitation method

ABSTRACT

Nickel ferrite nanoparticles were synthesized using Iron (III) nitrate and nickel nitrate as the starting materials along with the hydrazine hydrate via co-precipitation process and the final product obtained calcined at 700 °C. The structural and optical properties of the synthesised product were determined using various characterization techniques viz. UV–visible spectrometry, X-ray diffractometer (XRD), transmission electron microscopy (TEM), Field Emission Scanning Electron Microscopy (FE-SEM) and vibrating sample magnetometer (VSM). The $NiFe_2O_4$ nanoparticles showed absorption at ~ 356 nm corresponds to band gap of 4.1 eV. The elemental analysis was carried out using X – ray Fluorescence (XRF) and Energy Dispersive Spectroscopy (EDS). The synthesized $NiFe_2O_4$ were 10–15 nm in size, and exhibited high saturation magnetization value of 72.66 emu/g.

Selection and peer-review under responsibility of the scientific committee of the Integrative Nanotechnology Perspective for Multidisciplinary Applications - 2022.

1. Introduction

In recent years, magnetic particle synthesis has received a lot of attention due to its prospective applications in high-density magnetic recording and magnetic fluids [1,2]. In terms of applications in high-density magnetic recording media and magnetic fluids, the production of nanosized magnetic particles is being thoroughly researched [3]. Ferrites with good dielectric properties are used in a wide range of applications, from microwaves to radio waves. Because of its high electrical resistivity and low magnetic coercivity [4], Ni^{2+} ferrite is a technologically relevant material for uses in the megahertz frequency range. Nickel ferrite has been extensively investigated due to its unique inverse spinel structure, electrical and magnetic properties, and a wide range of uses in electronic devices and microwave adsorbents. In $NiFe_2O_4$, Fe^{3+} ions can easily shift between the octahedral (Oh) and tetrahedral (Td) sites, with Fe^{3+} occupying the Td site and Fe^{3+} and Ni^{2+} occupying the Oh site. The stable structural configuration allows it to endure the Fe^{3+} to Fe^{2+} reaction in a reducing environment. Because of its redox characteristics (LPG), $NiFe_2O_4$ can be used as a gas sensor material to detect reducing gases, such as liquefied petroleum gas, as a result [5–7].

In overview, several chemical processes, such as precipitation, sonochemical procedure, polymeric precursor approaches, mechanical alloying, pulsed wire discharge, shock wave, reverse micelles, hydrothermal and ultrasonically aided hydrothermal processes, have tremendous disadvantages over physical approaches, including lower costs, room-temperature reactions, and the ability to produce huge quantities, have all been used to make $NiFe_2O_4$ nanocrystalline [8]. Various shaped $NiFe_2O_4$ nanoparticles, such as fibre, sheet, ribbon, and rod, have been synthesised using organic gel–thermal decomposition, electrospinning combined with sol–gel technology [9–10], porous anodic aluminium oxide (AAO) templates, mechano-chemical method, and microemulsion method, among other methods, reverse phase micelles [10], hydrothermal micelles [11], and co–precipitation method [12] and also [13].

In the observation of magnetic materials, nanocrystalline spinel ferrites with the formula MFe_2O_4 (M = Ni, Zn, Mn, Co, Mg, etc.) execute high-density magnetic storage media, MRI contrast agents, colour imaging, ferro-fluids, high frequency devices, magnetic

* Corresponding author.
E-mail addresses: kazisubiya123@gmail.com (S. Kazi), saliinamdar@gmail.com (S. Inamdar), sarnikaryp@gmail.com (Y. sarnikar), dhanrajkamble1109@gmail.com (D. Kamble), rmtigote.chemobad@bamu.ac.in (R. Tigote).

https://doi.org/10.1016/j.matpr.2022.09.590
2214-7853/
Selection and peer-review under responsibility of the scientific committee of the Integrative Nanotechnology Perspective for Multidisciplinary Applications - 2022.

refrigerators, catalysts, and microwave devices, etc. investigation. The state of the properties of these magnetic nanoparticles are mostly determined by their size and method of production. Their most prevalent feature is their super-paramagnetic behaviour, which is characterised by a decrease in saturation magnetization as compared to the bulk material [14–18]. Researchers are particularly interested in nickel ferrite ($NiFe_2O_4$) because of its significant magneto-crystalline anisotropy, high saturation magnetization [19–20], and distinctive magnetic structure [21]. Gas and biosensors [22], sensors, magnetic fluids [23], catalysts, magnetic storage systems, photo magnetic materials [24], site-specific drug delivery [25–26], magnetic resonance imaging, and microwave devices are some of the important applications of $NiFe_2O_4$ nano material [27–28]. Nickel ferrite ($NiFe_2O_4$) exhibits ferromagnetic characteristics that are closer to dipole relaxation than ferromagnetic resonance and the magnetic moments of anti-parallel spins between Ni^{2+} ions at octahedral sites and Fe^{3+} ions at tetrahedral sites give nickel ferrite ($NiFe_2O_4$) its ferromagnetic characteristics [29–32].

A group of soft ferrite materials characterised by high magnetic permeability and research dealing with their other physical properties, such as optical and magnetic properties, is part of the continuation of Nickel Ferrite. These materials are commonly used in various applications, viz. computer memory chips for microwave devices, magnetic recording media, radio frequency, coil processing, transformer cores, rod antennas, and many telecommunications and electronic engineering branches [33–35].

In this work, we have synthesised nickel ferrite using hydrazine hydrate to afford their new fluorescence properties using a modified co-precipitation method. It is recognised as an environmentally friendly procedure and the characterization done using powder X-ray diffraction, scanning electron microscopy (SEM), transmission electron microscopy (TEM), elemental analysis using EDS, XRF, and the determination of $NiFe_2O_4$ nanoparticles' magnetic behaviour are all covered in this paper.

2. Materials and methods

2.1. Materials

Chemicals with high purity were purchased from Himedia and used without further purification. Distilled water was used for all the experiments. Iron nitrate ($Fe(NO_3)_3{\cdot}9H_2O$), nickel nitrate ($Ni(NO_3)_26H_2O$), and hydrazine hydrate ($NH_2.NH_2{\cdot}H_2O$) are the starting materials.

2.2. Synthesis of $NiFe_2O_4$ nanomaterials

A $NiFe_2O_4$ nanomaterial sample was prepared via a co-precipitation synthesis route by using a modified method of Suresh Sagadevan [39]. In a typical synthesis, 40 mL (2 M) solutions of iron nitrate ($Fe(NO_3)_39H_2O$) and 40 mL (1 M) solutions of nickel nitrate ($Ni(NO_3)_26H_2O$) were prepared and vigorously mixed under magnetic stirring for 1 h at 40 °C. Then a solution of 1 M hydrazine hydrate was added drop by drop into the reaction mixture to maintain pH = 8 and a blackish brown colored crude $NiFe_2O_4$ precipitate was formed. Finally, the $NiFe_2O_4$ nanoparticles were separated by the filtration method and dried at room temperature for 24 hrs. The acquired crude material was calcinated at 700 °C for 4 h to afford a fine powder by the grinding method.

3. Result and discussion

The structural properties of $NiFe_2O_4$ nanoparticles were defined by the XRD method using the Cu Kα (0.154 nm) radiation X-ray diffractometer to produce diffraction patterns at the scanning angle between 20 ° to 80 ° degrees for powder crystalline samples. The optical study was performed using Ellico's Double Beam Spectrophotometer. The nanocrystalline microstructure and particle size were calculated from Transmission Electron Microscopy (TEM) images obtained at an accelerating voltage of 200 kV using an electron microscope. The Field Emission Scanning Electron Microscopy (FE – SEM) and Energy Dispersive X – Ray Spectroscopy by using Carl Zeiss Model Supra 55 Germany and Bruker XFlash6l30 Germany, respectively. In order to eliminate any impu-

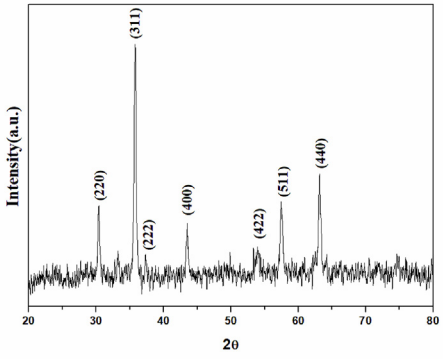

Fig. 1. XRD Spectrum of $NiFe_2O_4$ Nanoparticles.

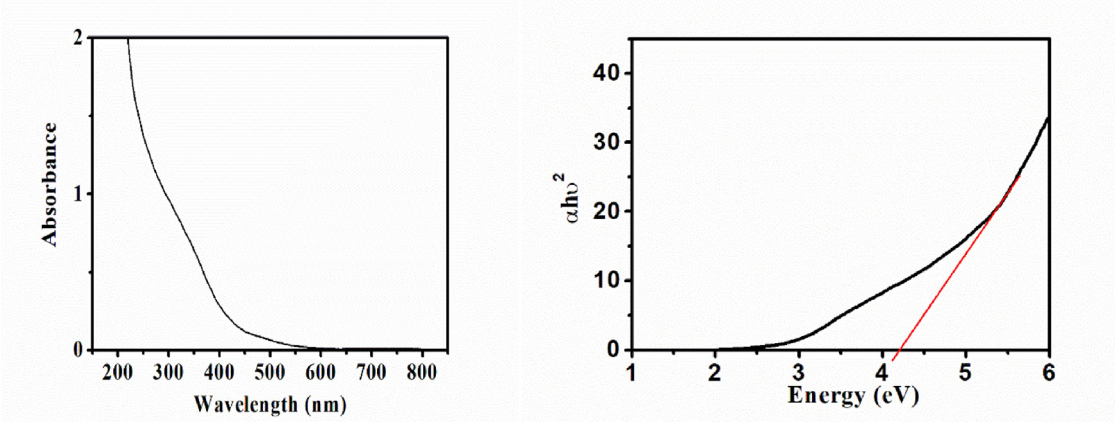

Fig. 2. a) UV–Visible spectrum of $NiFe_2O_4$ Nanomaterial; b) TAUC plot for optical band gap of $NiFe_2O_4$ Nanomaterial.

rities, present in the samples, the TGA analysis was performed in the 30–900 °C temperature range.

3.1. X- ray diffraction studies

In the powder XRD analysis, the peaks are found with planes (*hkl*) 220, 311, 222, 400, 321, 422, 511, and 440, which exhibits a BCC structure with spinel structure as shown in Fig. 1. This diffraction pattern shows that there are no extra peaks along the sample peak, confirming that the sample contains no impurity. Using the Debye-Scherrer formula for this data, we calculate the average particle size as 29 nm and the interplanar distance (d), lattice constant (a), volume (V) and X-ray density (d_x) are 1.31, 2.63, 18.32, and 1.83×10^{-24} respectively. The hopping lengths of octahedral sites

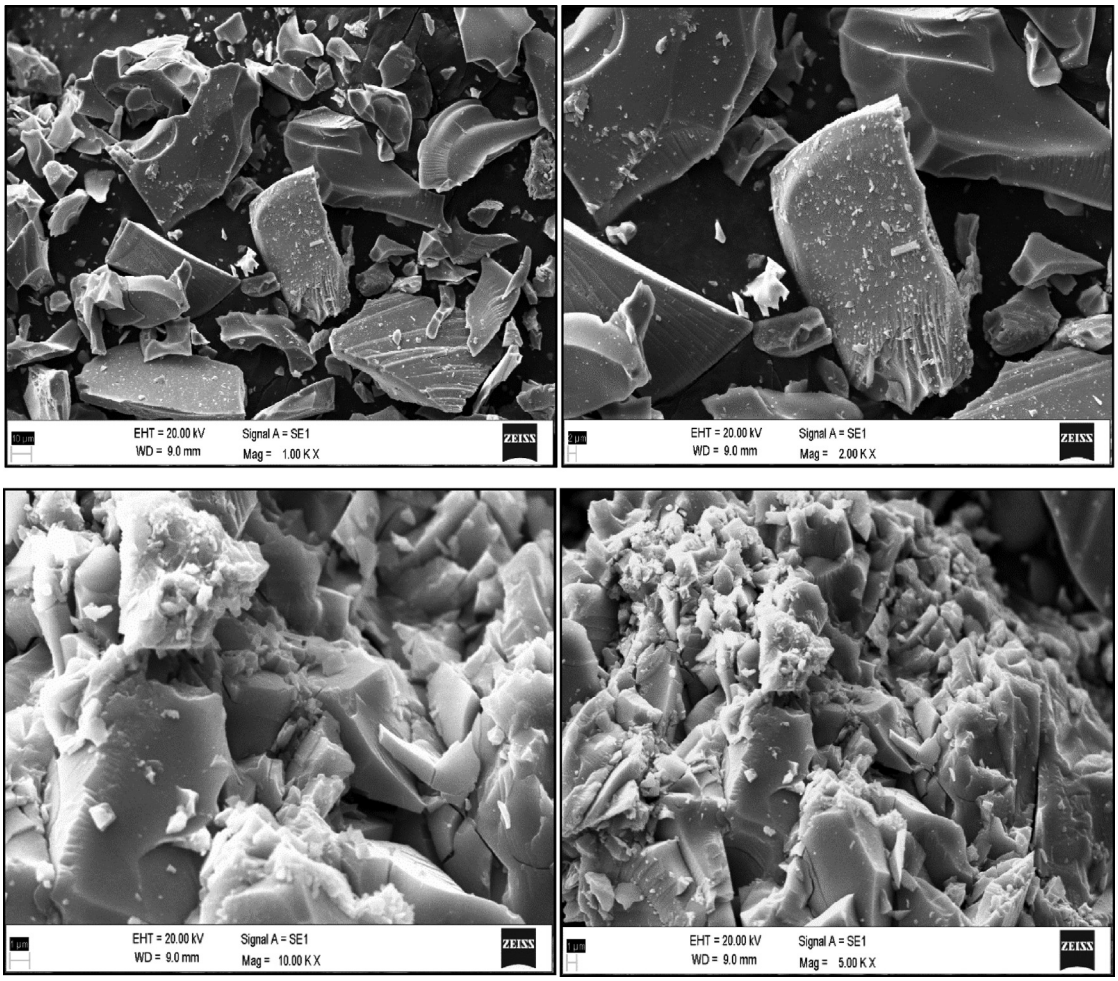

Fig. 3. FE-SEM of $NiFe_2O_4$ Nanomaterial.

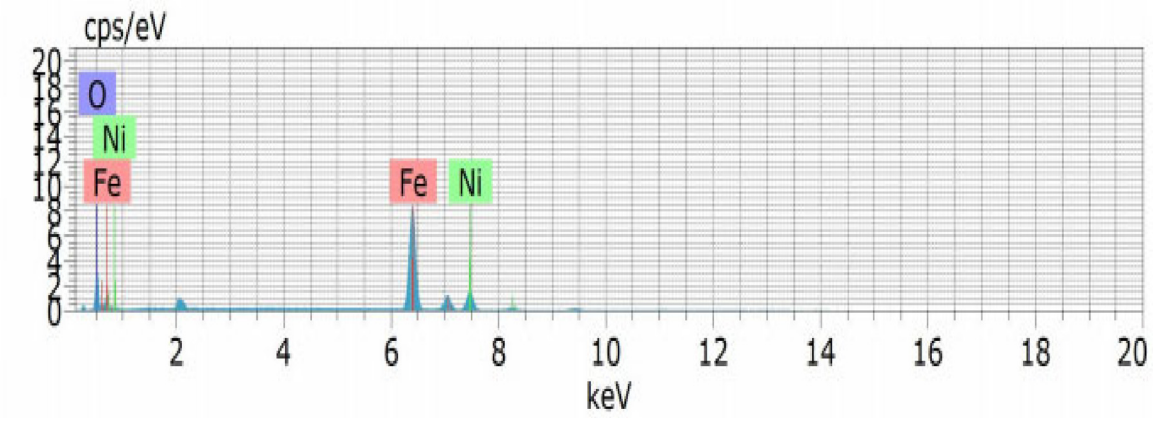

Fig. 4. EDS spectrum of $NiFe_2O_4$ Nanomaterial.

and tetrahedral sites are 1.139 and 0.930, respectively, corelate with Y. Kinemuchi [5].

3.2. Optical studies

Given the low solubility of transitional elements in organic solvents and water, the sample should be left in an acid solution for the study of the UV–Visible spectrum. The molecule undergoes an electrical transformation in the region of the electromagnetic spectrum. The maximum wavelength absorption charge transition band (~356 nm) is shown in Fig. 2a. The direct band gap was calculated by using the direct TAUC method [36]. The TAUC plot of $(\alpha h\mu)^2$ vs photoenergy ($h\mu$), where $h\mu$ is the photon energy, α is the absorption coefficient, which can be obtained from the scattering and reflectance spectra, gives the transition energy of 4.1 eV as shown in Fig. 2b [37].

Table 1
Atomic and Elemental composition of $NiFe_2O_4$ Nanomaterial.

Element	Atomic %	Weight %
Ni	25.04	32.18
Fe	47.64	58.26
O	27.28	9.55

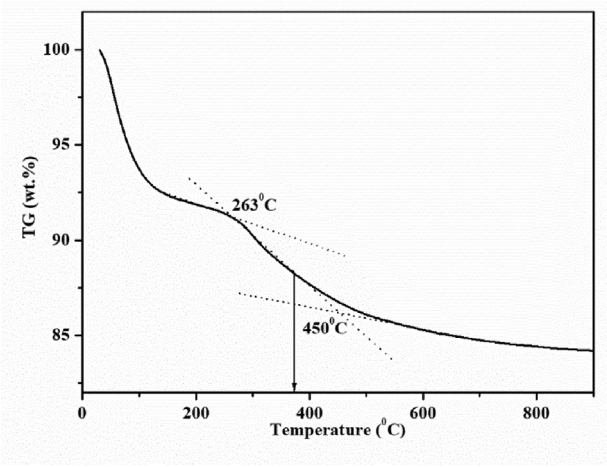

Fig. 5. TGA plot for $NiFe_2O_4$ Nanomaterial.

3.3. Scanning electron microscopy and elemental analysis

The morphology study of nanoparticles using SEM shows that the synthesised nanoparticles are quasispheroidal and that their size is less than 100 nm, which suggests that the nano-dimensional catalysts are synthesized. This result also supports the knowledge obtained from XRD. As shown in Fig. 3, the results obtained from the above measurements of the prepared ferrite nanoparticles by the co-precipitation method are 29 nm. It was observed that the morphology of the ferrite nanoparticles by SEM data was confirmed by XRD and demonstrated a uniform size distribution.

The morphology of the majority of nanoparticles is quasi-spherical in the SEM picture. Another SEM image determination is related to the particle size, i.e., the nano dimension exhibits the formed particles (less than 100 nm) as analogous to that reported by K. Egizbek [26]. The Ni Ferrite Nanoparticles EDS spectrum is shown in Fig. 4. The atomic and elemental compositions are tabulated in Table 1.

3.4. Thermal analysis

A TGA measurement was used to determine the mass fraction of $NiFe_2O_4$ shown in Fig. 5. The TGA analysis was used to remove impurities from the sample, from 30 °C to 200 °C. The initial loss is due to the initial breakdown of the complex and evaporation

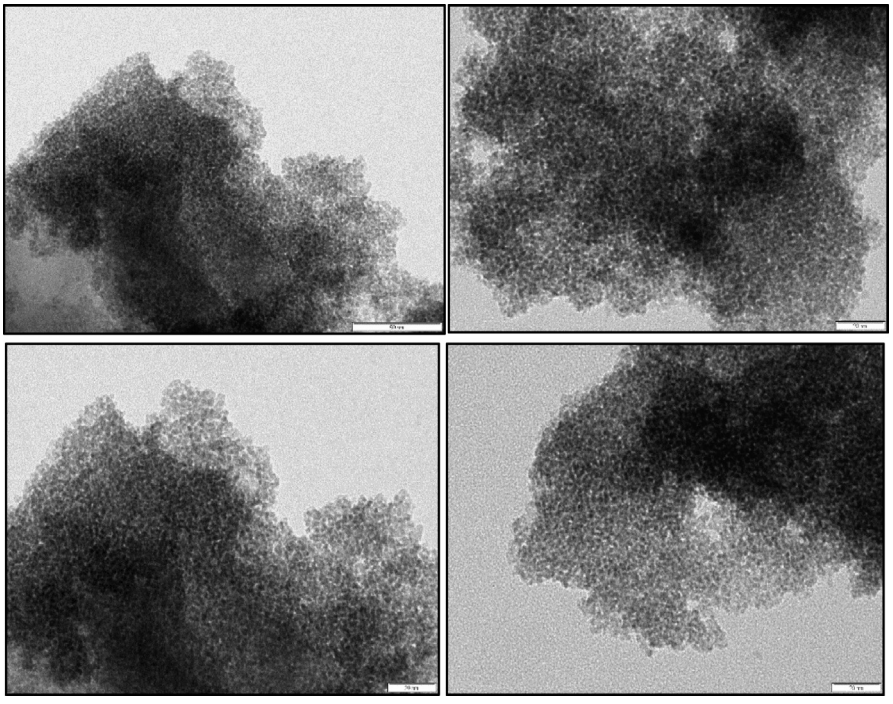

Fig. 6. TEM images of $NiFe_2O_4$ nanoparticles (scale bar is 50 nm for all images).

of the absorbed water. The second loss is due to further decomposition of inorganic salts and traces of hydrazine hydrate [38]. Then, above 450 °C stable oxides at 900 °C. The first stage of weight loss is 5.5 % due to the breakdown of the complex and evaporation of the absorbed water. The second weight loss is 2.3 % as a result of the decomposition of organic matter and the decomposition of inorganic salts and traces of hydrazine hydrate [39]. No weight loss is found beyond 450 °C, indicating the formation of $NiFe_2O_4$ nanoparticles. 263 °C is the initial decomposition temperature and 450 °C is the final decomposition temperature. The average of both decomposing materials shows the thermal stability of the material.

3.5. Transmission electron microscopy

Fig. 6 shows the TEM image of $NiFe_2O_4$ nanomaterial showing an aggregated particle-type structure. The particle size distribution ranges from 10 to 15 nm for $NiFe_2O_4$ nanomaterial. These nanoparticles are synthesised by a simple co-precipitation technique similar to that of Suresh Sagadevan [39].

3.6. Magnetic studies

The $NiFe_2O_4$ nanomaterial was synthesised by using the simple co-precipitation method. The magnetic property of the synthesised

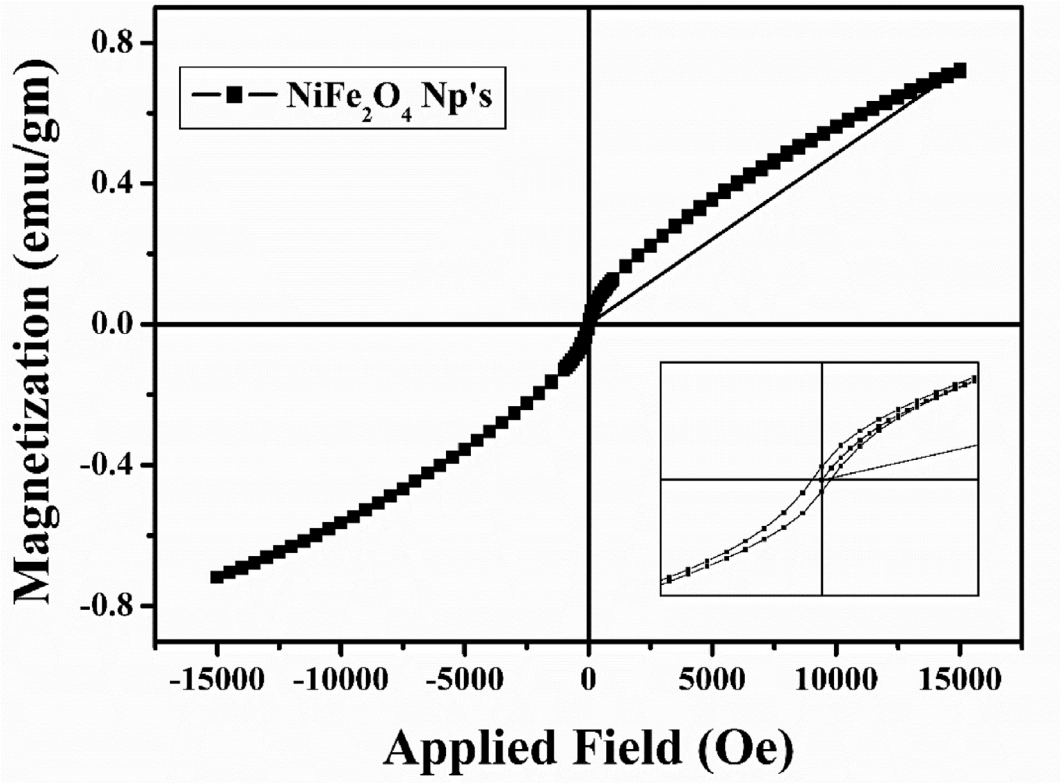

Fig. 7. Magnetic Hysteresis loop of $NiFe_2O_4$ nanomaterial.

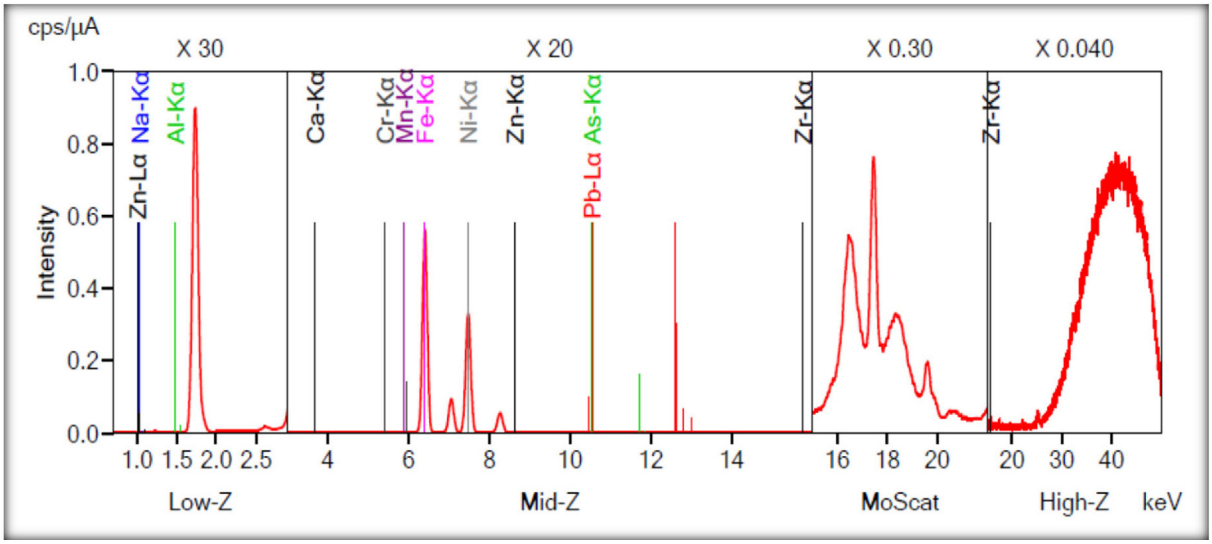

Fig. 8. XRF plot of $NiFe_2O_4$ nanomaterial.

Table 2
XRF Data of $NiFe_2O_4$ Nanomaterial.

Materials	Elemental Composition		Total
	NiO	Fe_2O_3	
$NiFe_2O_4$	26.62	73.38	100 %

spinel ferrite nanoparticles was measured by a Vibrating Sample Magnetometer (VSM). Fig. 7 shows the magnetic hysteresis curve of the $NiFe_2O_4$ sample. The product was observed to exhibit ferromagnetic behaviour. The saturation magnetization (Ms), the coercivity (Hc), remanence magnetization (Mr), Bohr Magnetization (μB) and anisotropy constant (K_1) are 72.66, 2.627, 2.348, 3.049, and 95.43 (erg/cm^3), respectively, and have been determined from the M−H loop. The sample is mainly due to the substitution of the part of Ni^{2+} in octahedral sites by Fe^{3+} with a higher magnetic moment. The saturation magnetization of the sample is higher due to the spin counting effect of the smaller crystalline size. It is reported that [39] the magnetic properties of the material have been believed to be dependent on the particle size, shape, and magnetization direction.

3.7. X-ray Fluorescence

The surface composition of $NiFe_2O_4$ was also studied by the X-ray Fluorescence technique where the emission spectra are recorded as shown in the following Fig. 8. The total elemental composition was analysed by using this technique. The elemental composition as shown in Table 2**.**

4. Conclusion

The nickel-doped spinel ferrite nanocrystals were synthesized using an environmentally friendly process of co-precipitation. The synthesized spinel ferrite $NiFe_2O_4$ nanocrystals were calcinated at temperature of 700 °C. The formation of the $NiFe_2O_4$ nanocrystals were verified by XRD, UV–Visible Spectrum, EDS, XRF, TGA, FE-SEM, TEM, and VSM studies. Nickel ferrite displayed super-paramagnetic behaviour and increased saturation magnetization. It showed the cubic spinel structure with particle size of 10–15 nm, confirmed by the XRD and TEM techniques. Elemental analysis of the $NiFe_2O_4$ nanoparticles were done using the EDS and XRF studies. Optical study showed maximum absorption at ∼ 356 nm with 4.1 eV band gap value. The quasispheroidal structure was obtained by FE-SEM images. Synthesized material showed high thermal stability, about 85 % even on heating over 800 °C temperature.

CRediT authorship contribution statement

Subiya Kazi: Investigation, Writing – original draft. **Radhakrishnan Tigote:** Supervision.

Declaration of Competing Interest

The authors declare that they have no known competing financial interests or personal relationships that could have appeared to influence the work reported in this paper.

Acknowledgements

We wish to thank the Department of Chemistry, Dr. Babasaheb Ambedkar Marathwada University Sub-Campus, Osmanabad for providing facilities to carry out this research work and the UGC, New Delhi for providing financial assistance under the Maulana Azad National Fellowship to Miss. Subiya K. Kazi. (F1-17.1/2014-15/MANF-2014-15-MUS-MAH-47640/(SA-III/Website)).

References

[1] S.H. Chen, S.C. Chang, I.N. Lin, J. Magn. Magn. Mater. 209 (2000) 193–196, https://doi.org/10.1016/S0304-8853(99)00685-X.
[2] Y. Shi, J. Ding, X. Liu, J. Wang, *Journal of Magnetism and Magnetic Materials* **1999**, *205*, 249-254.https://doi.org/10.1016/S0304-8853(99)00504-1.
[3] C. Bradley, *Regulated Rivers: Research & Management* **2001**, *17*, 295-295. https://doi.org/10.1002/rrr.637.
[4] Y. Kinemuchi, K. Ishizaka, H. Suematsu, W. Jiang, K. Yatsui, *Thin Solid Films* **2002**, *407*, 109-113.https://doi.org/10.1016/j.matpr.2019.07.298.
[5] S.S. Jadhav, S.E. Shirsath, B.G. Toksha, S.M. Patange, D.R. Shengule, K.M. Jadhav, Phys. B 405 (2010) 2610–2614, https://doi.org/10.1016/j.physb.2010.03.008.
[6] S. Feng, W. Yang, Z. Wang, Mater. Sci. Eng.: B 176 (2011) 1509–1512, https://doi.org/10.1007/s12274-020-2626-y.
[7] G.D. Price, S.L. Price, J.K. Burdett, Phys. Chem. Miner. 8 (1982) 69–76, https://doi.org/10.1007/bf00309016.
[8] M. Singh, S.P. Sud, Mater. Sci. Eng.: B 83 (2001) 180–184, https://doi.org/10.1016/S0921-5107(01)00514-1.
[9] P. Sivakumar, R. Ramesh, A. Ramanand, S. Ponnusamy, C. Muthamizhchelvan, Mater. Lett. 65 (2011) 483–485, https://doi.org/10.1016/j.matlet.2010.10.056.
[10] D. Zhang, X. Zhang, X. Ni, J. Song, H. Zheng, Chem. Phys. Lett. 426 (2006) 120–123, https://doi.org/10.1016/j.cplett.2006.05.100.
[11] C. Liu, B. Zou, A. Rondinone, Z. Zhang, J. Phys. Chem. B 104 (2000) 1141–1145, https://doi.org/10.17350/HJSE19030000154.
[12] P. Sivakumar, R. Ramesh, A. Ramanand, S. Ponnusamy, C. Muthamizhchelvan, Appl. Surf. Sci. 258 (2012) 6648–6652, https://doi.org/10.1016/j.apsusc.2012.03.099.
[13] P. Sivakumar, R. Ramesh, A. Ramanand, S. Ponnusamy, C. Muthamizhchelvan, Mater. Lett. 66 (2012) 314–317, https://doi.org/10.1016/j.matlet.2011.09.005.
[14] X. Qi, J. Zhou, Z. Yue, Z. Gui, L. Li, Mater. Sci. Eng.: B 99 (2003) 278–281, https://doi.org/10.1016/S0921-5107(02)00524-X.
[15] H.M. Widatallah, I.A. Al-Omari, A.M. Gismelseed, O.A. Yassin, A.D. Al-Rawas, M. E. Elzain, A.A. Yousif, O.A. Osman, Hyperfine Interact. 169 (2006) 1325–1329, https://doi.org/10.1007/s10751-008-9773-y.
[16] V.A. Fedorov, V.A. Ganshin, Y.N. Korkishko, Phys. Status Solidi (a) 139 (1993) 9–65, https://doi.org/10.1002/pssa.2211390102.
[17] P.J. van der Zaag, M. Kolenbrander, M.T. Rekveldt, J. Appl. Phys. 83 (1998) 6870–6872, https://doi.org/10.1063/1.367562.
[18] K. Takadate, Y. Yamamoto, A. Makino, T. Yamaguchi, I. Sasada, J. Appl. Phys. 83 (1998) 6861–6863, https://doi.org/10.1063/1.367765.
[19] R.V. Penney, J. Phys. Chem. Solids 25 (1964) 335–345, https://doi.org/10.1016/0022-3697(64)90112-X.
[20] P. Sivakumar, R. Ramesh, A. Ramanand, S. Ponnusamy, C. Muthamizhchelvan, J. Alloy. Compd. 563 (2013) 6–11, https://doi.org/10.1016/j.jallcom.2013.02.077.
[21] D. Yang, M.J. Campolongo, T.N. Nhi Tran, R.C.H. Ruiz, J.S. Kahn, D. Luo, WIREs Nanomed. Nanobiotechnol. 2 (2010) 648–669, https://doi.org/10.1166/jnn.2010.1722.
[22] B. Zeynizadeh, I. Mohammadzadeh, Z. Shokri, S. Ali Hosseini, J. Colloid Interface Sci. 500 (2017) 285–293, https://doi.org/10.1080/17518253.2019.1711202.
[23] W.E. Pottker, R. Ono, M.A. Cobos, A. Hernando, J.F.D.F. Araujo, A.C.O. Bruno, S.A. Lourenço, E. Longo, F.A. La Porta, Ceram. Int. 44 (2018) 17290–17297, https://doi.org/10.1021/acsomega.1c04079.
[24] C. Thirupathy, S. Cathrin Lims, S. John Sundaram, A.H. Mahmoud, K. Kaviyarasu, J. King Saud Univ. – Sci. 32 (2020) 1612–1618. https://www.researchgate.net/deref/https%3A%2F%2Fdoi.org%2F10.1016%2Fj.ceramint.2021.07.274.
[25] K. Egizbek, A. L. Kozlovskiy, K. Ludzik, M. V. Zdorovets, I. V. Korolkov, B. Marciniak, J. M, D. Chudoba, A. Nazarova, R. Kontek, *Ceramics International* **2020**, *46*, 16548-16555. https://doi.org/10.3390/molecules26020457
[26] T. Abbas, Y. Khan, M. Ahmad, S. Anwar, Solid State Commun. 82 (1992) 701–703, https://doi.org/10.1016/0038-1098(92)90064-G.
[27] E. C. Snelling, Butterworths, London; Boston, **1988**. http://books.google.com/books?id=yRNTAAAAMAAJ.
[28] Z. V.T, V. Tsakaloudi, E. Papazoglou, *Journal of Electroceramics* **2003**, *11*, 107-117. https://doi.org/10.1023/B:JECR.0000011216.01346.03
[29] M. Schaefer, G. Dietzmann, H. Wirth, J. Magn. Magn. Mater. 101 (1991) 95–96, https://doi.org/10.1016/0304-8853(91)90689-8.
[30] J.A.T. Taylor, S.T. Reczek, A. Rosen, American Ceramic Society, Westerville, OH (United States), United States, 1995.
[31] M. Rozman, M. Drofenik, J. Am. Ceram. Soc. 81 (1998) 1757–1764, https://doi.org/10.1111/j.1151-2916.1998.tb02545.x.
[32] R. Arulmurugan, G. Vaidyanathan, S. Sendhilnathan, B. Jeyadevan, J. Magn. Magn. Mater. 298 (2006) 83–94, https://doi.org/10.1016/j.jmmm.2005.03.002.
[33] S.R. Ahmed, S.B. Ogale, G.C. Papaefthymiou, R. Ramesh, P. Kofinas, Appl. Phys. Lett. 80 (2002) 1616–1618, https://doi.org/10.1063/1.5040890.
[34] D.L. Huber, Small 1 (2005) 482–501, https://doi.org/10.1002/smll.200500006.
[35] S.T. Hoseini, S. Khademolhoseini, J. Mater. Sci.: Mater. Electron. 27 (2016), https://doi.org/10.1007/s10854-016-4514-5.

[36] M.H. Habibi, F. Fakhri, J. Mater. Sci.: Mater. Electron. 28 (2017) 13455–13463, https://doi.org/10.1007/s10854-017-7184-z.
[37] A. Al-Hunaiti, A. Ghazzy, N. Sweidan, Q. Mohaidat, I. Bsoul, S. Mahmood, T. Hussein, Nanomaterials (2021) 11, https://doi.org/10.3390/nano11041010.
[38] P. Sivagurunathan, S.R. Gibin, J. Mater. Sci.: Mater. Electron. 27 (2016) 2601–2607, https://doi.org/10.1007/s10854-015-4065-1.
[39] S. Sagadevan, Chowdhury, Zaira Zaman and Rafique, Rahman F, *Materials Research [online]* **2018**, *21*, 533. http://dx.doi.org/10.1016/j.rinp.2018.12.058